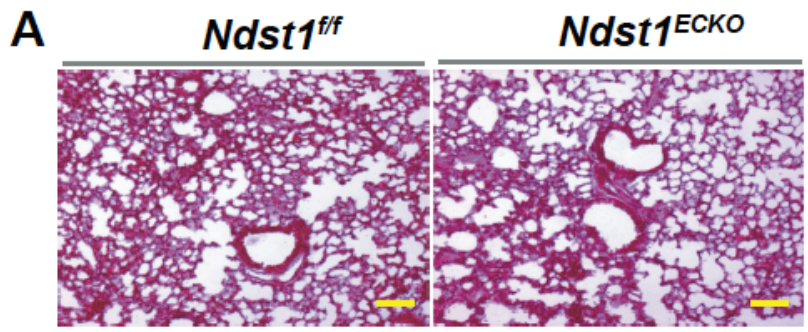
A
Ndst1f/f
Ndst1ECKO

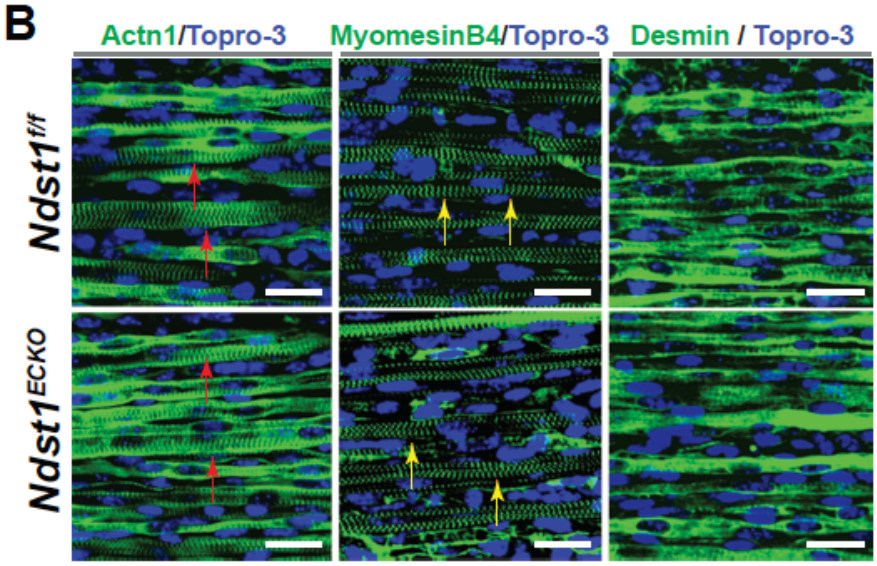
B
Actn1/Topro-3
MyomesinB4/Topro-3
Desmin / Topro-3
Ndst1f/f
Ndst1ECKO

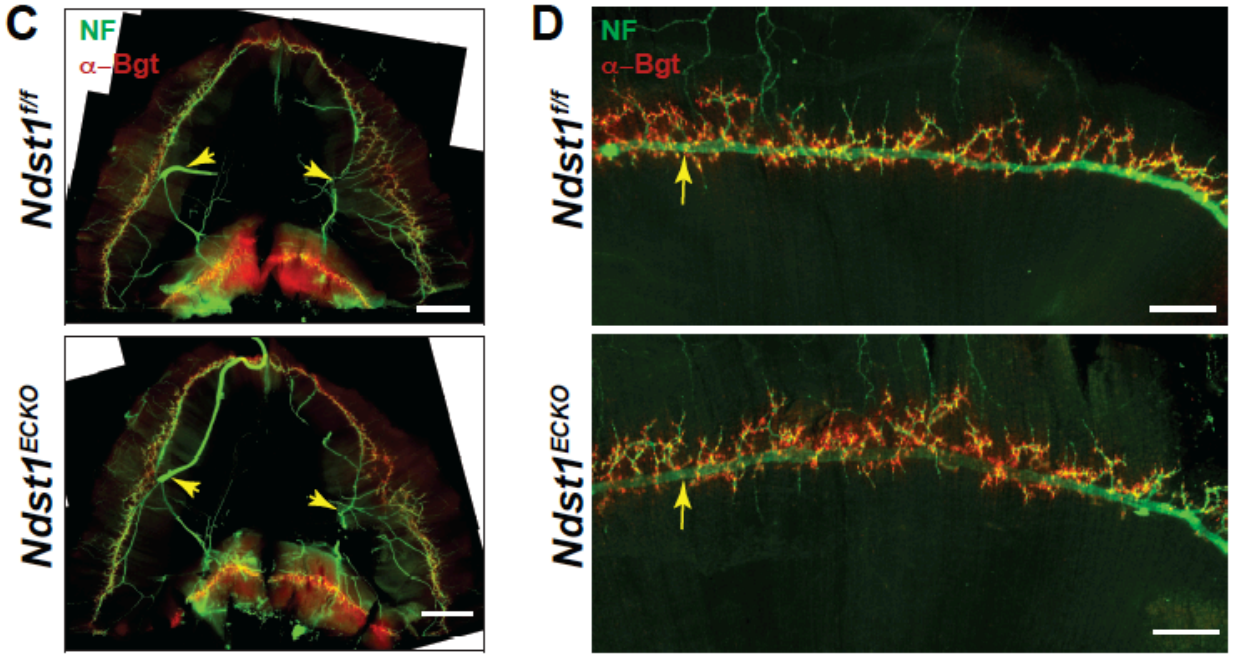
C
NF
α–Bgt
Ndst1f/f
Ndst1ECKO
D
NF
α–Bgt
Ndst1f/f
Ndst1ECKO

Supplemental Figure 1. Loss of endothelial Ndst1 did not affect lung structure, and muscular and phrenic neural patterning in the diaphragm. **(A)**. H&E staining of E18.5 lung tissue sections showed that the pulmonary architecture of *Ndst1*^{ECKO} and *Ndst1*$^{f/f}$ littermate controls were similar, demonstrating that *Ndst1*^{ECKO} mice had normal lung development. **(B)**. Whole-mount co-immunofluorescence staining of E15.5 diaphragmatic muscle using anti-Actinin1 (Actn1, marker of Z-band, red arrows), anti-Myomesin B4 (marker of M-band, yellow arrows) or anti-Desmin antibody. Images are representative of 3-5 mice per group. **(C,D)**. Whole-mount co-immunofluorescence staining of E18.5 diaphragms with antibodies against neurofilament (NF) to label motor axons and α-bungarotoxin (α-Bgt) to label postsynaptic acetylcholine receptors (AChRs). Representative of 6-8 mice per group. The overall branching pattern of the phrenic nerve and the position of phrenic nerve entry points (arrow heads) are not altered in *Ndst1*^{ECKO} mice compared to *Ndst1*$^{f/f}$ littermate controls (C). Motor axons form a tightly fasciculated main intramuscular nerve (arrows), and individual motor axons innervate postsynaptic AChR clusters adjacent to the main nerve trunk in both *Ndst1*^{ECKO} mice and *Ndst1*$^{f/f}$ controls (D). Scale bars: 0.2 mm (**A**; **D**); 20 μm (**B**); 1 mm (**C**).

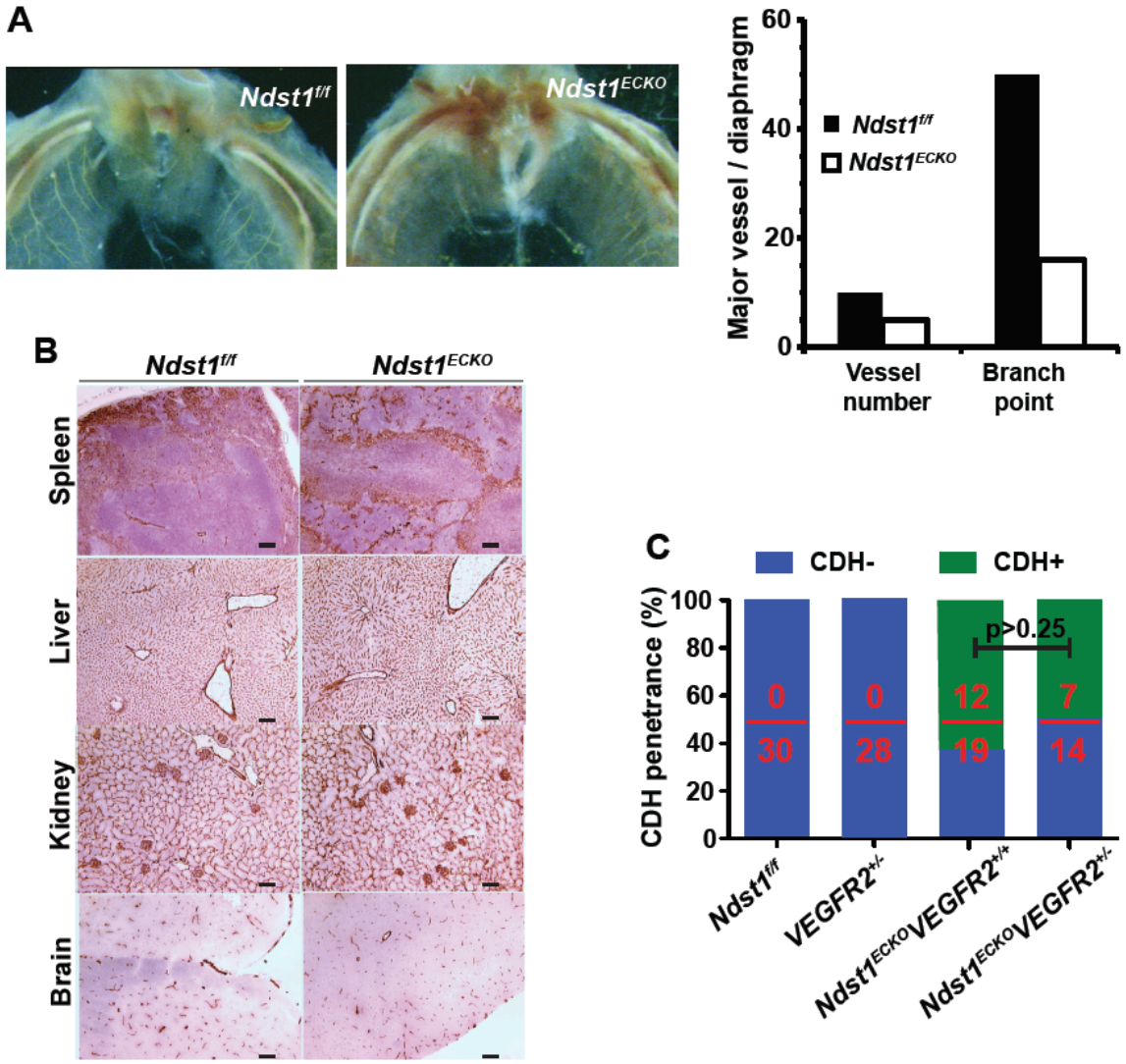

Supplemental Figure 2. *Ndst1*^{ECKO} mice show abnormal vascular development only in diaphragm and no genetic interaction of endothelial Ndst1 with VEGFR2 in CDH aetiogenesis. **(A)**. Major vessel in diaphragm. Major vessels were defined as the ones that branched from the phrenic vessel into diaphragm, and their branch points were defined as the 1st-3rd degree branches stemming from the major vessels. Quantification showed that both major vessels and their branch points were reduced in the anterior region of *Ndst1*^{ECKO} diaphragm (n=5-6). **(B)**. Tissue sections of E18.5 mouse embryos were stained with anti-PECAM-1 antibody and the general vascular structure in spleen, liver, kidney and brain were examined. No obvious differences were observed between *Ndst1*^{ECKO} and their *Ndst1*$^{f/f}$ littermate control (n=3-4). **(C)**. Genetic interaction of endothelial Ndst1 with VEGFR2 in CDH. CDH penetrance of control (*Ndst1*$^{f/f}$), *VEGFR2*$^{+/-}$, *Ndst1*^{ECKO}*VEGFR2*$^{+/+}$ and *Ndst1*^{ECKO}*VEGFR2*$^{+/-}$ mice were examined. CDH did not occur in *VEGFR2*$^{+/-}$ mice. The bottom numbers show the total animals examined and the numbers on the top indicate the CDH positive animals. Statistical analysis was carried out by $\chi 2$ – test. Scale bars: 250 μm (**B**).

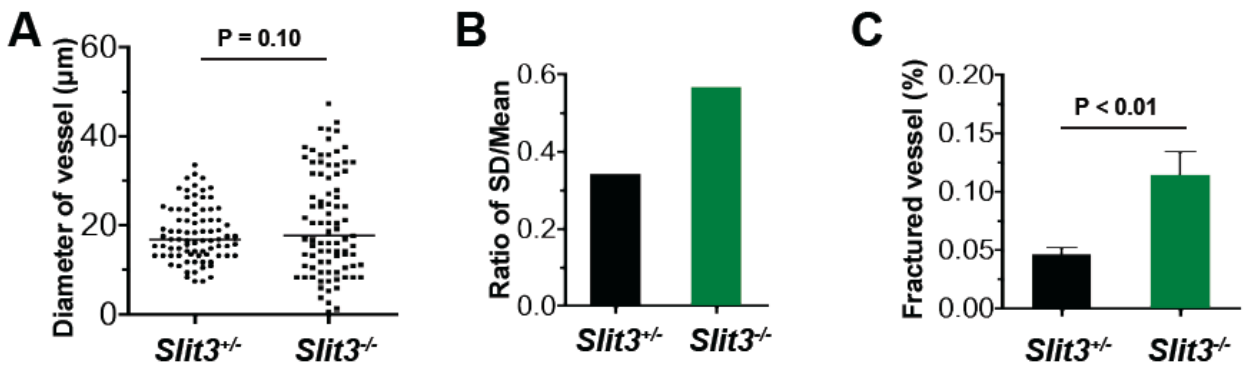

Supplemental Figure 3. Vascular defect in *Slit3*$^{-/-}$ E16.5 diaphragm, including increased variation of vessel diameter **(A, B)** and more fractured vessels **(C)**.

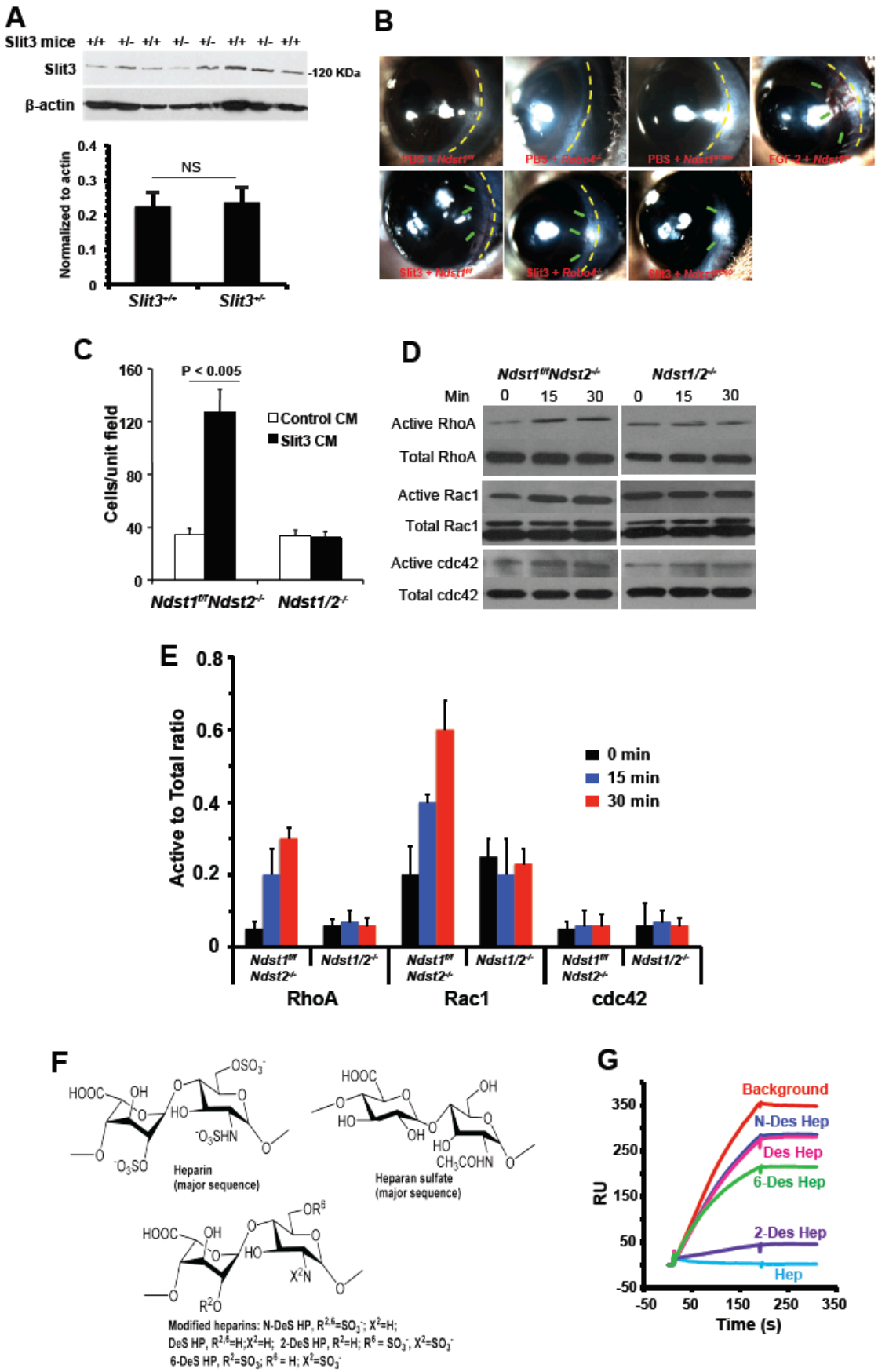
A
Slit3 mice +/+ +/- +/+ +/- +/- +/+ +/- +/+
Slit3
-120 KDa
β-actin
Normalized to actin
NS
Slit3+/+
Slit3+/-
B
PBS + Ndst1fl/fl
PBS + Robo4-/-
PBS + Ndst1fl/fl/Cre
FGF-2 + Ndst1fl/fl
Slit3 + Ndst1fl/fl
Slit3 + Robo4-/-
C
P < 0.005
Control CM
Slit3 CM
Cells/unit field
Ndst1fl/flNdst2-/-
Ndst1/2-/-
D
Ndst1fl/flNdst2-/-
Ndst1/2-/-
Min 0 15 30 0 15 30
Active RhoA
Total RhoA
Active Rac1
Total Rac1
Active cdc42
Total cdc42
E
Active to Total ratio
0 min
15 min
30 min
Ndst1fl/fl Ndst2-/-
Ndst1/2-/-
RhoA
Rac1
cdc42
F
Heparin (major sequence)
Heparan sulfate (major sequence)
Modified heparins: N-DeS HP, R2,6=SO3-; X2=H;
DeS HP, R2,6=H;X2=H; 2-DeS HP, R2=H; R6 = SO3-, X2=SO3-
6-DeS HP, R2=SO3; R6 = H; X2=SO3-
G
Background
N-Des Hep
Des Hep
6-Des Hep
2-Des Hep
Hep
RU
Time (s)

Supplemental Figure 4. Slit3 expression, angiogenic activity, RhoGTPases activation and Slit3 binding to heparinoids. **(A)**. Slit3 expression in diaphragm. E17.5 diaphragms were collected and homogenized individually. The homogenates were analyzed by Western blot probing with anti-Slit3 antibody. Quantification showed that the Slit3 protein intensity in *Slit3*$^{+/-}$ and littermate *Slit3*$^{+/+}$ diaphragms were not different. The results are presented as average + SEM (n = 4, *P* > 0.40). NS, not significant. **(B)**. Slit3-induced corneal angiogenesis was disrupted in *Robo4*$^{-/-}$ and *Ndst1*^{ECKO} mice. Hydro pellets containing FGF-2 (4.8 no) or Slit3 (1.3 no) were implanted into micro pockets generated in mouse corneas. The pellets with balanced buffers were used as a negative control. On day 5, the corneal revascularization response to test factors was photographed and quantified. To reduce experimental variation, each mouse was implanted in one eye with the test-factor or in the other eye with control pellets. Representative pictures are shown from 5-7 mice for each group. **(C)**. Slit3-induced lung EC migration depended on endothelial HS. Slit3-induced EC migration in Boyden Chambers was carried out with Slit3-containing conditioned medium (CM) or CM collected from mock-transected stable N2A cells. The *Ndst1*$^{f/f}$*Ndst2*$^{-/-}$ mouse lung ECs posses normal HS structure, whereas the *Ndst1/2*$^{-/-}$ daughter line produces very poorly sulfated HS with dramatically reduced legend-binding capacity. The data was summarized from three independent experiments and are presented as mean ± SD. **(D,E)**. Slit3-induced Robo4 signaling depends on endothelial HS. *Ndst1*$^{f/f}$*Ndst2*$^{-/-}$ and *Ndst1/2*$^{-/-}$ mouse lung ECs were stimulated with Slit3, and the downstream signaling of Robo4 (RhoA, Rac1 and Cdc42) was examined. Activation of Rac1 and RhoA in *Ndst1/2*$^{-/-}$ ECs was significantly reduced compared to *Ndst1*$^{f/f}$*Ndst2*$^{-/-}$ ECs. **(F)**. Chemical structure of major sequences of heparin, HS and modified-heparins. **(G)**. Loss of *N*-sulfation abolished binding of heparin to Slit3. The Slit3 protein (10 nM) was premixed with 1000 nM heparin (Hep), fully-desulfated-heparin (Des-Hep), *N*-desulfated-heparin (N-Des-Hep), 6-*O*-desulfated-heparin (6-Des-Hep) or 2-*O*-desulfated-heparin (2-Des-Hep) and then the mixture was injected over heparin coated CM5 chips. Des-Hep and N-Des-Hep, and to a lesser extent 6-Des-Hep, lost their potency to inhibit Slit3 binding to immobilized heparin. The SPR sensorgram shown is representative of three experiments.

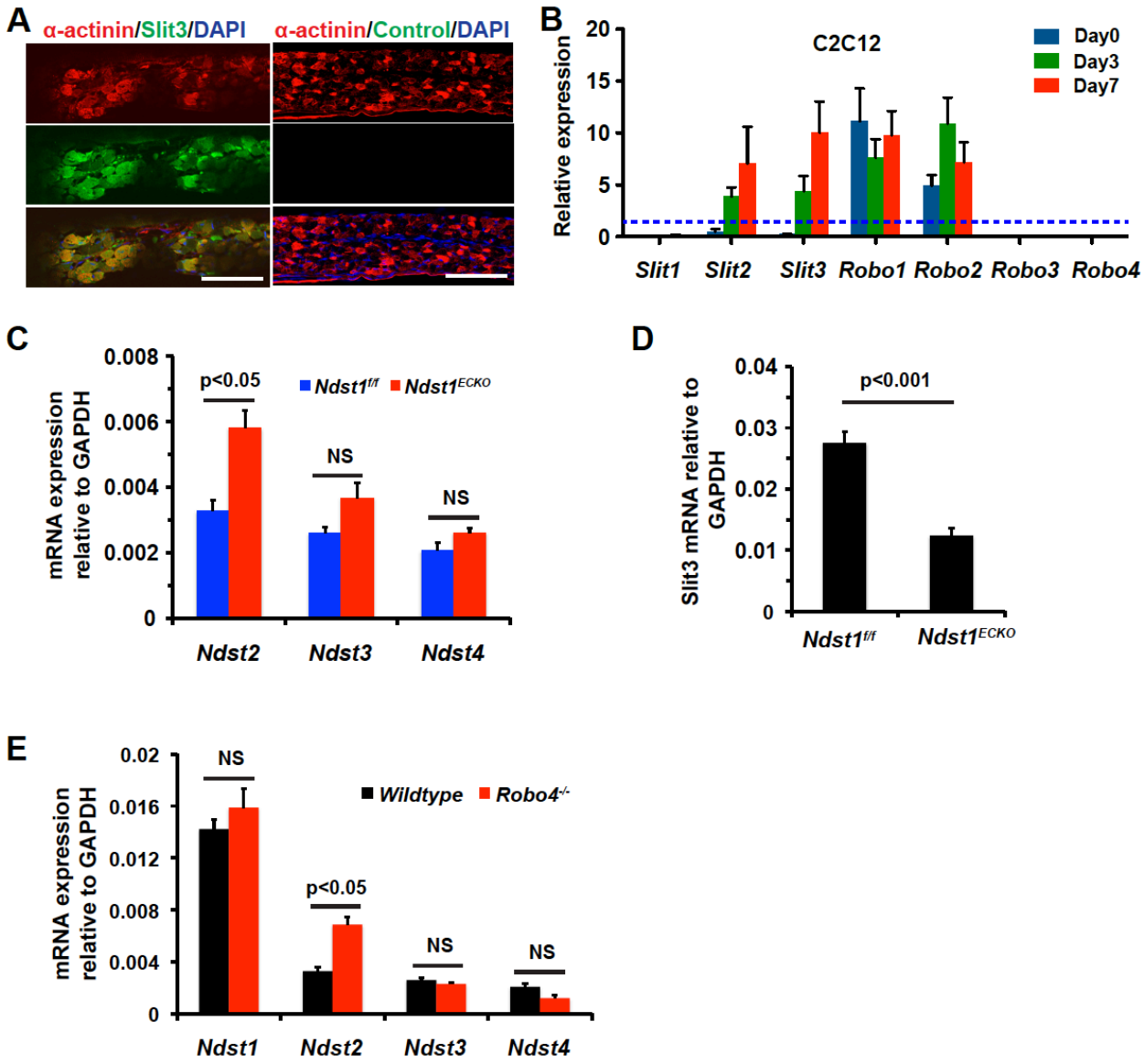

Supplemental Figure 5. Slit3 binding to diaphragm muscle cells, and Slit/Robo expression in myoblast and diaphragmatic ECs. **(A).** Slit3 binds to diaphragmatic muscle cell. Biotinylated-Slit3 were diluted with 10 fold of PBS and incubated with P0 embryo cryosection for 1 hour at room temperature, followed by fixation in 4% PFA for 20 min. The diaphragmatic muscle fibers were revealed by anti-α-actinin antibody. **(B)**. *Slit2-3* and *Robo1-2* express in C2C12 differentiated myofibers. Undifferentiated (Day 0) and differentiated C2C12 (Day 3 and 7) were collected for RT-qPCR analysis. The expression levels of *Slits* and *Robos* are presented relatively to Ct35 (blue line). **(C-E).** Expression of *Ndsts* and *Slit3* in passage 0 primary diaphragmatic ECs. NS, not significant. Scale bars: 40 μm (**A**).

Table 1. Primer sequences

Gene	Forward	Reverse
Slit1	5`-aggtgcaaaagggcgaat-3`	5`-cgagagggtacaggcaggt-3`
Slit2	5`-tcgagccagctatgacacc-3`	5`-ttccatcattgattgtctccac-3`
Slit3	5`-gccacctcagtgagaacctc-3`	5`-tgtccctcaaagcccaga-3`
Robo1	5`-agggaagcctacgcagatg-3`	5`-tggacagtgggcgattttat-3`
Robo2	5`-gaaattttgggcgtggaga-3`	5`-gtcgctgttttatccccttg-3`
Robo3	5`-gcagcgctcaaccctagt-3`	5`-cttctggcccaactcttgac-3`
Robo4	5`-aatggtgtcatccgtggttac-3`	5`-agttggcagcaggcaatg-3`
Ndst1	5`-ggaatccagtcgcttcaaat-3`	5`-gtctgtgagtgtgggcatgt-3`
Ndst2	5`-gggattcctacggatctgg-3`	5`-tagagctgcgagtggatgg-3`
Ndst3	5`-ggtgtttgtggagagccagt-3`	5`-gaaccggatggattctagca-3`
Ndst4	5`-tcaggtcaccagcactgaag-3`	5`-gaatgaagcccttcctgtacc-3`
GAPDH	5`-aactttggcattgtggaagg-3`	5`-atgcagggatgatgttctgg-3`